Graphene Oxide Flakes as a Cellular Adhesive: Prevention of Reactive Oxygen Species Mediated Death of Implanted Cells for Cardiac Repair

Jooyeon Park,[†,#] Bokyoung Kim,[‡,#] Jin Han,[†] Jaewon Oh,[‡] Subeom Park,[⊥] Seungmi Ryu,[§] Subin Jung,[‡] Jung-Youn Shin,[†] Beom Seob Lee,[‡] Byung Hee Hong,[⊥] Donghoon Choi,[*,‡] and Byung-Soo Kim[*,†,§,∥]

[†]School of Chemical and Biological Engineering, Seoul National University, Seoul 151-744, Republic of Korea, [‡]Severance Integrative Research Institute for Cerebral & Cardiovascular Diseases, Yonsei University Health System, Seoul 120-752, Republic of Korea, [§]Interdisciplinary Program of Bioengineering, Seoul National University, Seoul 151-744, Republic of Korea, [⊥]Department of Chemistry, Seoul National University, Seoul 151-747, Republic of Korea, and [∥]Bio-MAX Institute, Institute of Chemical Processes, Seoul National University, Seoul 151-744, Republic of Korea. [#]These authors contributed equally to this work.

ABSTRACT Mesenchymal stem cell (MSC) implantation has emerged as a potential therapy for myocardial infarction (MI). However, the poor survival of MSCs implanted to treat MI has significantly limited the therapeutic efficacy of this approach. This poor survival is primarily due to reactive oxygen species (ROS) generated in the ischemic myocardium after the restoration of blood flow. ROS primarily causes the death of implanted MSCs by inhibiting the adhesion of the MSCs to extracellular matrices at the lesion site (*i.e.*, anoikis). In this study, we proposed the use of graphene oxide (GO) flakes to protect the implanted MSCs from ROS-mediated death and thereby improve the therapeutic efficacy of the MSCs. GO can adsorb extracellular matrix (ECM) proteins. The survival of MSCs, which had adhered to ECM protein-adsorbed GO flakes and were subsequently exposed to ROS *in vitro* or implanted into the ischemia-damaged and reperfused myocardium, significantly exceeded that of unmodified MSCs. Furthermore, the MSC engraftment improved by the adhesion of MSCs to GO flakes prior to implantation enhanced the paracrine secretion from the MSCs following MSC implantation, which in turn promoted cardiac tissue repair and cardiac function restoration. This study demonstrates that GO can effectively improve the engraftment and therapeutic efficacy of MSCs used to repair the injury of ROS-abundant ischemia and reperfusion by protecting implanted cells from anoikis.

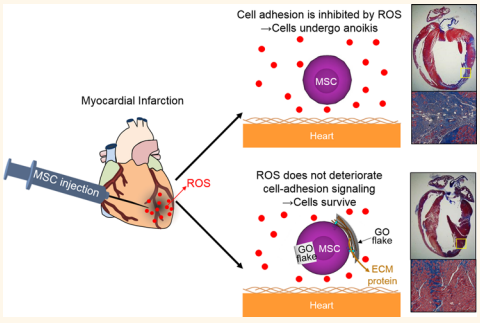

KEYWORDS: anoikis · cell implantation · graphene oxide · myocardial infarction · reactive oxygen species

Cardiovascular disease continues to be one of the major causes of death around the world.[1,2] Serum deprivation and hypoxia due to restricted blood flow in myocardial infarction (MI) lead to cardiac cell death.[3] Previous studies have demonstrated that the implantation of mesenchymal stem cells (MSCs) can contribute to heart repair mainly by secreting paracrine factors.[4,5] However, the therapeutic benefit of MSC implantation remains very limited due to the poor engraftment and survival of implanted MSCs.[6,7] One of the main causes for the poor survival is reactive oxygen species (ROS) generated in the infarcted region after the restoration of blood flow.[8,9] ROS in the infarcted area hinder the adhesion of MSCs to the extracellular matrices (ECMs) of the heart tissue by disrupting focal contacts.[10] The loss of MSC adhesion induces the MSC apoptosis, which is known as anoikis,[11] thereby limiting the therapeutic efficacy of MSCs implanted for cardiac repair.[12]

Graphene oxide (GO) is a two-dimensional hydrophilic nanosheet composed of carbon, oxygen, and hydrogen.[13,14] GO has drawn much attention for its biomedical applications, such as bioimaging,[15,16] drug delivery,[17] gene delivery,[18,19] and tissue engineering.[20,21] The functional groups on the GO surface enable GO to efficiently adsorb proteins from the serum.[22] GO can adsorb proteins though hydrophobic interactions, electrostatic forces, and hydrogen bonding.[23] The proteins from the serum

* Address correspondence to byungskim@snu.ac.kr, cdhlyj@yuhs.ac.

Received for review December 15, 2014 and accepted April 28, 2015.

Published online April 28, 2015
10.1021/nn507149w

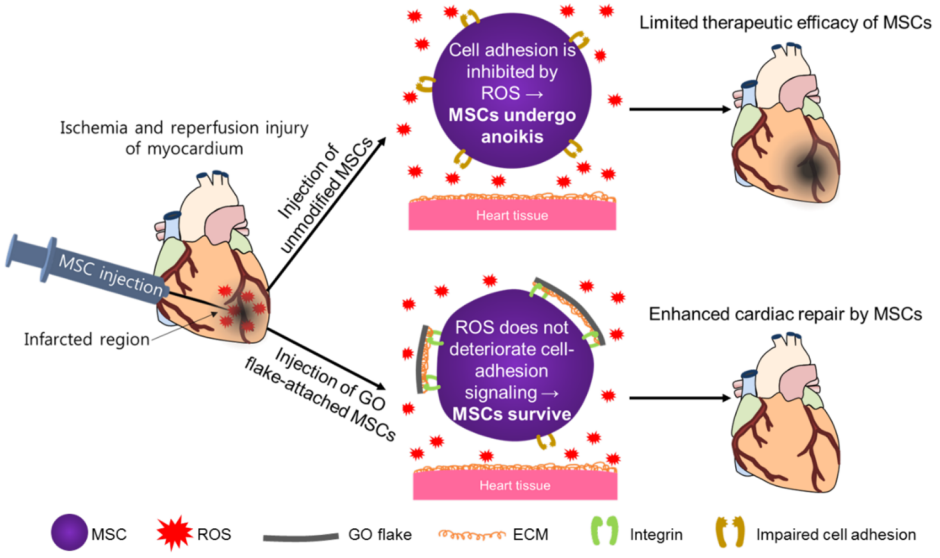

Figure 1. Schematic representation of the effects of GO adhesion on the MSCs prior to MSC implantation on the therapeutic efficacy of the MSCs injected into the infarcted myocardium. ROS, which are generated in the ischemic myocardium after the restoration of blood flow, limit the adhesion of implanted MSCs to ECM of the myocardium, which causes the apoptosis of the MSCs due to lack of MSC−ECM interaction (*i.e.*, anoikis; see Figure 4a for more detail). Therefore, allowing MSCs to adhere to GO flakes prior to implantation, which provides the cell−ECM interaction between MSCs and the ECM adsorbed on GO flakes, allows MSCs to escape anoikis when implanted into ROS-abundant injured heart tissue.

contained in cell culture media include ECM proteins.[24] The adsorption of ECM proteins on GO promotes cell adhesion to GO.[23] Therefore, we hypothesized that the attachment of GO to MSCs (MSC-GO) may preserve the cell−ECM interactions even when cell adhesion to the heart tissue damaged by MI is impaired. While unmodified MSCs would undergo anoikis when implanted into the infarcted region due to hindered cell adhesion by ROS in ischemia and reperfusion injury, MSCs adhering to GO prior to implantation would be able to escape anoikis due to cell−ECM interactions between MSCs and the ECM proteins adsorbed on GO (Figure 1). To test this hypothesis, we first investigated whether MSC adhesion to GO attenuates ROS-mediated deterioration in adhesion, viability, and paracrine factor secretion of MSCs *in vitro*. The signaling mechanisms involved in the adhesion and apoptosis of MSCs were also analyzed. Next, we investigated whether the implantation of MSC-GO to the reperfused MI region improved the survival, growth factor secretion, and therapeutic efficacy of implanted MSCs by examining angiogenesis, cardiac repair, and heart functions. Here, we introduce a new application of GO as a cellular adhesive to improve the therapeutic efficacy of MSC implantation therapy for the treatment of ROS-abundant ischemia and reperfusion injury.

RESULTS AND DISCUSSION

Characterization of GO Flakes. The atomic force microscopy (AFM) image of GO flakes showed that the height of flakes was ~1.5 nm, indicating that the GO flakes are monolayer (Figure 2a). The size distribution of GO flakes showed that the size of GO flakes ranged from 1 to 6 μm (Figure 2a). Figure 2b shows a representative transmission electron microscopy (TEM) image, and Figure 2c shows the corresponding selected area electron diffraction (SAED) patterns of a GO flake. The six-fold rotational symmetry of SAED patterns showed graphene-like crystallinity (Figure 2c).[25] The Fourier transform infrared spectroscopy (FTIR) spectrum of GO (Figure 2d) showed intense peaks corresponding to hydroxyl groups at 3355 and 1630 cm^{-1}. A strong band at 1225 cm^{-1} was assigned to the C−OH stretching vibrations, and the bands at 1414 and 1055 cm^{-1} were attributed to the C−O stretching vibrations. The FTIR spectra showed peaks that were the same as previously reported FTIR spectra of typical GO.[25] Therefore, there was no sign of organic pollutants in GO flakes. The inductively coupled plasma mass spectrometry (ICP-MS) analyses of GO flakes detected negligible amounts[26] of heavy metal pollutants: Ni (0.004 mg/L), Cr (0.010 mg/L), Mn (0.036 mg/L), and Fe (0.118 mg/L). In addition, we confirmed that the Raman spectrum of GO included two broad peaks, which are known as the G and D bands (1590 and 1350 cm^{-1}, respectively) (Figure 2e).

GO Adhesion on MSCs. The cytotoxicity of GO flakes was examined by measuring the viability of MSCs after being treated with various concentrations of GO flakes because previous study showed that GO may be cytotoxic in a dose-dependent manner.[27] The analysis of the MSC viability, as assessed using a cell counting kit-8, indicated that the cytotoxicity of GO flakes was not significant at concentrations below 20 μg/mL (Figure 2f), which coincides with the results of a

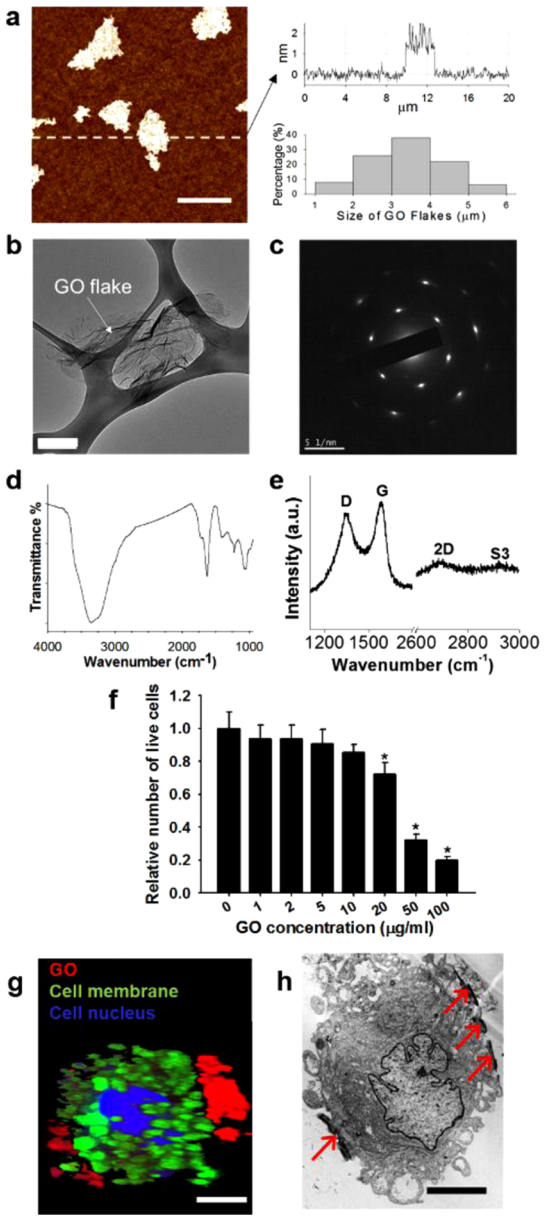

Figure 2. Characterization of GO flakes and their adhesion on MSCs. (a) Tapping-mode AFM image of GO flakes, the height along the line shown in the AFM image, and the size distribution of GO flakes. Scale bar, 4 μm. (b) TEM image of GO flake. Scale bar, 1 μm. (c) SAED pattern, (d) FTIR spectra, and (e) Raman spectra of GO flakes. (f) Viability of MSCs cultured for 3 days with various concentrations of GO flakes added to the culture. *$p < 0.05$ compared to any group; $n = 3$. (g) Adhesion of DiI (red)-labeled GO flakes on MSCs. The MSC nucleus was stained with DAPI (blue). The MSC membrane was stained with PKH67 (green). Scale bar, 20 μm. (h) TEM image of GO flakes (arrows) attached to the MSC surface. Scale bar, 20 μm.

previous study.[28] Therefore, we used GO flakes at 10 μg/mL for further experiments.

The attachment of GO flakes to MSCs was examined by fluorescence staining and TEM. Although GO is known to quench fluorescence,[29] GO sheets can be labeled with DiI *via* adsorption,[30] and increasing the DiI concentration can overcome the fluorescence quenching.[31] Therefore, we labeled GO with high concentrations of DiI to avoid fluorescence quenching to examine GO flake adhesion to MSCs. The DiI labeling of GO flakes, 4′-6-diamidino-2-phenylindole (DAPI) staining of cell nuclei, and PKH67 staining of the cell membrane demonstrated that GO flakes attached to the MSC membrane (Figure 2g). The TEM image of MSC-GO also showed the adherence of several GO flakes on the membrane of a MSC (Figure 2h). The relative area of GO adherent to MSCs, as quantified using TEM images, was 25.6 ± 10.1% of the cell surface area. Although there were several studies that showed cellular uptake of GO nanoparticles (20−300 nm in size),[32,33] there was no sign of GO flake internalization by MSCs in this study (Figure 2g,h). This may be due to the microscale size of GO flakes (1−6 μm, Figure 2a) as particle sizes can influence the cellular uptake of the particles.[32,34]

A previous study demonstrated that GO can effectively adsorb proteins *via* hydrophobic interactions, electrostatic forces, and hydrogen bonding.[23] Therefore, it would be possible to control the protein adsorption by modifying GO chemistry. It has previously been reported that the protein adsorption can be controlled by the oxygen content of GO.[23] For example, GO shows enhanced adsorption of proteins such as fibroblast growth factor (FGF) and fibronectin (FN) compared to that of reduced GO.[23] In the present study, GO prepared by the modified Hummer's method was used as it can effectively facilitate the cell adhesion.[20]

The adsorption of ECM proteins on GO can induce cell adhesion to GO.[35] Therefore, as an example, we analyzed the capability of GO flakes to adsorb FN, a kind of ECM protein. The adsorption of FN to GO flakes immersed in serum-containing medium was examined. The results demonstrated that FN from the culture medium was adsorbed to GO, while no FN was detected on GO flakes immersed in phosphate buffered saline (PBS), which was used as a control (Supporting Information Figure S1).

Enhanced Cell Adhesion and Survival under ROS Conditions *in Vitro*. Paracrine factors secreted from MSCs can promote cardiac regeneration after MI.[36] High engraftment and survival rates of implanted MSCs are necessary for a sustained supply of paracrine factors.[37] However, a burst of ROS is generated at the lesion site after blood restoration in the infarcted region,[38] which significantly impairs the adhesion of implanted MSCs to the infarcted region and results in apoptosis of the MSCs caused by a loss of cell−ECM interaction. This lack of interaction leads to poor engraftment and survival of the implanted MSCs.[12]

To determine whether MSC adhesion to GO flakes can attenuate ROS-mediated cell anoikis, we examined the cell adhesion to culture surfaces and viabilities of MSCs and MSC-GO in the presence of ROS. To simulate the ROS levels produced by ischemia and reperfusion

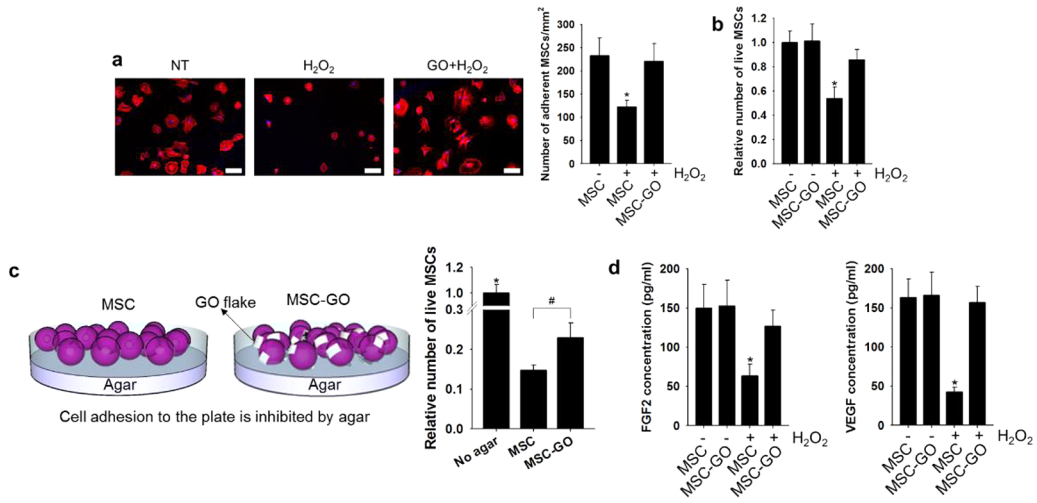

Figure 3. Attenuation of ROS-mediated deterioration in adhesion, viability, and paracrine factor secretion of MSCs by MSC adhesion to GO flakes *in vitro*. ROS were generated in the culture by adding H_2O_2. (a) Adhesion of MSCs and MSC-GO to the culture plates 90 min after culture in the medium containing 0 (no treatment, NT) or 200 μM H_2O_2 as evaluated by F-actin staining. Scale bars, 10 μm. (b) Relative number of live cells assessed 24 h after the culture of MSCs and MSC-GO in medium containing 0 (NT) or 200 μM H_2O_2. (c) Viability of MSCs and MSC-GO when cultured on an agar plate, which completely inhibits cell adhesion. The result was compared with MSCs cultured in a culture plate without agar. H_2O_2 was not added to the culture for all groups. Importantly, the result indicates that GO flake adhesion to MSCs attenuates the anoikis of MSCs. (d) Amounts of FGF2 and VEGF secreted by MSCs and MSC-GO with or without H_2O_2. *$p < 0.05$ compared to any group; $^{\#}p < 0.05$; $n = 3$.

injury *in vitro*, hydrogen peroxide (H_2O_2), a common model of an exogenous ROS source, was added to the culture medium. First, the initial cell adhesion was visualized by staining filamentous actin (F-actin) with phalloidin. The F-actin staining showed that unmodified MSCs displayed a round morphology in the presence of ROS, and the number of adherent cells was significantly decreased, which demonstrated that their ability to adhere was significantly disrupted (Figure 3a). The impairment MSC adhesion by H_2O_2 was likely due to impaired integrin-mediated cell adhesion to ECM molecules.[39] Conversely, the morphology of MSC-GO was more spread out and similar to control MSCs, which were cultured in the absence of H_2O_2. This morphology, along with the number of adherent cells, demonstrated that these cells could more easily attach to the culture surface (Figure 3a), which may be due to decreased anoikis of MSC-GO, which retained the interactions with the ECM *via* their adhesion to the ECM-adsorbed GO flakes. The loss of cell−ECM interactions in unmodified MSCs led to anoikis. Therefore, the number of live cells significantly decreased when unmodified MSCs were exposed to ROS, while the adhesion of MSCs to GO could protect the cells from anoikis (Figure 3b).

To further examine whether GO flake adhesion to MSCs attenuates MSC anoikis, MSCs and MSC-GO were cultured on agar-coated plates. The culture plates were coated with agar to inhibit cell adhesion to the plate and mimic the *in vivo* condition of ischemia and reperfusion injury, in which cell adhesion to the heart tissue is disturbed by ROS.[12] After 24 h, only 15 ± 1% of the cells survived on the agar-coated plate compared to MSCs cultured on cell culture plates without agar coating (Figure 3c). The dramatic decrease in the cell survival rate was due to the inhibition of cell adhesion (*i.e.*, anoikis). Conversely, MSC adhesion to GO flakes significantly increased the survival rate (Figure 3c). This improved cell survival in MSC-GO was likely due to the cell−ECM interactions that result from MSCs adhering to the FN adsorbed to GO, which attenuated anoikis.

The enhanced cell survival of MSC-GO increased the secretion of paracrine factors *in vitro* (Figure 3d). Treating MSCs with ROS significantly reduced the secretion of FGF2 and vascular endothelial growth factor (VEGF), which are important paracrine angiogenic factors for ischemic tissue repair.[40,41] The reduced paracrine factor secretion may be due to the poor MSC survival after ROS treatment. Conversely, the amounts of FGF2 and VEGF secreted by MSC-GO in the presence of ROS were similar to those of MSCs and MSC-GO cultured without ROS (Figure 3d). These results suggest that the number of live MSCs can determine the amount of secreted paracrine factors.

Mechanism of Enhanced Cell Survival. The underlying mechanisms by which MSC adhesion to GO flakes prevents anoikis were examined by investigating the expression of cell-signaling molecules (Figure 4a). Both H_2O_2 treatment and cell detachment downregulate focal adhesion kinase (FAK) phosphorylation, which in turn enhances the activation of p38 and caspase-3, suggesting that ROS plays a role in cell anoikis.[42,43] To confirm that the disruption of cell adhesion by ROS produced these sequential cell-signaling events, we analyzed the expression of these signaling molecules in MSCs cultured in H_2O_2-containing medium. First, we

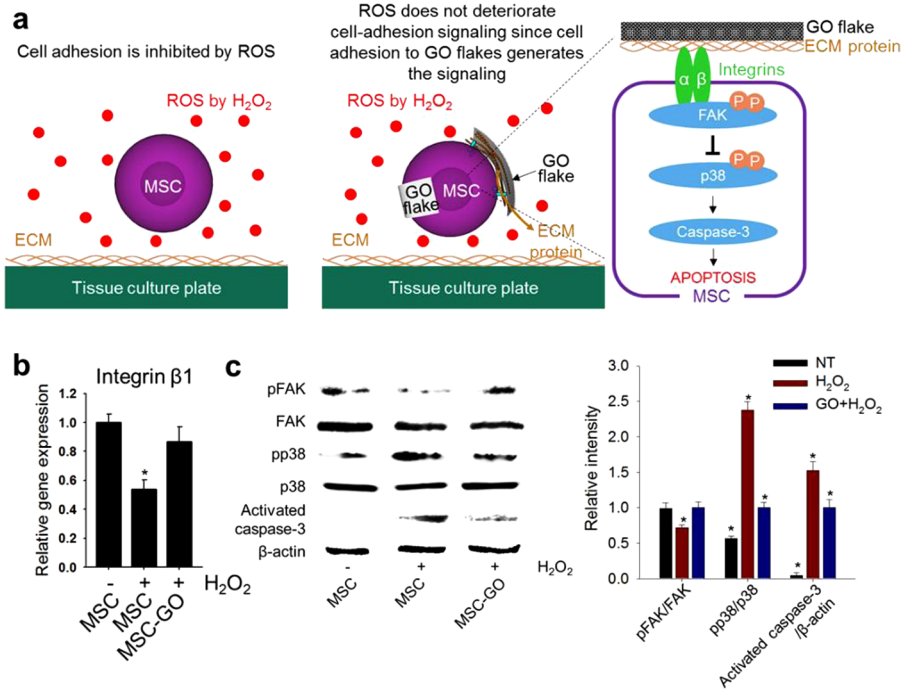

Figure 4. Attenuation of ROS-mediated deterioration in cell adhesion signaling and subsequent apoptosis of MSCs by MSC adhesion to GO flakes *in vitro*. (a) Schematic representation of anoikis signaling. (b) Expression of integrin β1 evaluated by qRT-PCR indicated that MSC adhesion to GO flakes avoids ROS-mediated deterioration in cell adhesion. (c) Expression of activated intracellular signaling molecules related to anoikis as evaluated by Western blot analyses. NT indicates no treatment (no H_2O_2). *$p < 0.05$ compared to any group; $n = 3$.

examined the expression of integrin β1, which is one of the major receptors by which cells can attach to ECM molecules.[44] The presence of H_2O_2 significantly downregulated the expression of integrin β1 (Figure 4b), indicating deteriorated cell adhesion to the culture plate. However, the downregulation of integrin β1 was rescued when MSCs were allowed to adhere to GO flakes because integrins could bind to the ECM proteins adsorbed on GO (Figure 4b). The downregulation of integrin β1 (*i.e.*, loss of cell adhesion) by ROS led to the downregulation of pFAK and the activation of p38 and caspase-3 (Figure 4c). Importantly, the impairment of cell adhesion and upregulation of apoptosis due to the exposure of MSCs to ROS were significantly ameliorated by allowing MSC to attach to GO (Figure 4c). This finding confirmed that GO flakes act as a cellular adhesive that provides surfaces for cell adhesion and protects MSCs from anoikis. However, MSC adhesion to GO flakes could not completely reduce the level of activated caspase-3 (Figure 4c), the activation of which leads to cell apoptosis. This phenomenon may be observed because ROS not only hinder cell adhesion but also induce cell apoptosis by regulating the phosphorylation of proteins related to apoptosis.[45]

To investigate whether the adsorption of ECM proteins on GO flakes induces integrin β1 expression for MSC adhesion to GO flakes and prevents apoptotic signaling, MSCs were cultured in a serum-free medium in the presence of ECM protein-adsorbed GO flakes and transferred to H_2O_2-containing medium. FN and vitronectin (VN) are main ECM proteins contained in serum that mediate cell adhesion.[46] Therefore, MSCs were incubated with FN-adsorbed GO [MSC+GO(FN)] and VN-adsorbed GO [MSC+GO(VN)] in serum-free medium prior to being placed under ROS conditions. MSC+GO(FN) and MSC+GO(VN) were compared with MSCs incubated with bare GO in serum-free medium (MSC+GO). After incubation in H_2O_2-containing medium, the expression of integrin β1 and the activation of p38 were analyzed. The results demonstrated that ECM protein (FN or VN)-adsorbed GO flakes promoted integrin β1 expression and prevented the activation of p38 in MSCs cultured under ROS conditions, while MSC+GO showed a similar tendency to MSCs alone under ROS conditions (Supporting Information Figure S2). Therefore, ECM proteins adsorbed on GO flakes played a major role in mediating MSC adhesion to GO and preventing ROS-mediated anoikis.

In order to determine whether free ECM proteins in serum-containing medium compete with ECM proteins adsorbed on GO flakes for their interactions with MSCs, we compared the adhesion of GO flakes on MSCs after incubating MSCs with ECM protein-adsorbed GO flakes in either serum-free medium or serum-containing medium for 24 h. The serum-containing medium has free ECM proteins. Unattached GO flakes were removed by being washed several times with PBS. ECM protein-adsorbed GO flakes were also incubated in serum-free medium and

serum-containing medium without MSCs for 24 h in order to confirm GO attachment to MSCs rather than the dish. The results demonstrated no attachment of GO flakes in the absence of MSCs (Supporting Information Figure S3), demonstrating GO flakes attached to MSCs rather than the dish. The presence of free ECM proteins in serum-containing medium did not influence the attachment of GO flakes to MSCs (Supporting Information Figure S3). Therefore, free ECM proteins in serum-containing medium did not compete with ECM proteins adsorbed on GO flakes to interact with MSCs.

A previous study reported that GO can reduce oxidative stress by scavenging hydroxyl radicals,[47] which could be a possible mechanism for the attenuation of ROS-mediated MSC death by GO flakes. In the present study, to address this possibility, we examined whether GO can reduce the level of ROS by incubating GO flakes in H_2O_2 (200 μM)-containing solution. After 24 h, the concentration of H_2O_2 in the solution incubated with GO flakes was 199.0 $\pm$ 1.1 μM, showing no significant difference compared with that (200 μM) of H_2O_2-containing solution without GO flakes. In addition, the 2′,7′-dichlorofluorescein diacetate (DCFDA) staining of intracellular ROS showed no difference between MSCs and MSC-GO cultured in H_2O_2-containing medium, demonstrating that the adhesion of GO flakes on MSCs did not alter the intracellular ROS in the MSCs (Supporting Information Figure S4). These results collectively demonstrate that GO flakes did not significantly scavenge ROS. This may be because the GO concentration (10 μg/mL) used in this study was much lower than the minimal GO concentration (100 μg/mL) that exhibits a significant ROS scavenging effect.[47] Furthermore, our data showed that only 25.6 $\pm$ 10.1% of MSC surfaces were covered with GO flakes (Figure 2h), suggesting that GO flakes could not act as a physical barrier to inhibit ROS from damaging MSCs. Therefore, the enhanced MSC survival under ROS conditions would be attributed to the interaction between GO flakes and MSCs rather than the ROS scavenging and physical barrier effects of GO flakes.

Enhanced Survival of MSCs Implanted in a Myocardial Ischemia and Reperfusion Model. The presence of ROS after reperfusion in the infarcted region is known to inhibit the adhesion of the implanted cells, which results in the apoptosis of the implanted cells due to a loss of cell adhesion (*i.e.*, anoikis).[12] To assess the engraftment of MSCs implanted in the infarcted region, we implanted MSCs labeled with DAPI prior to implantation. The initial engraftment of MSCs was assessed by counting the number of DAPI-labeled cells on day 3. The implantation of MSC-GO allowed a significantly larger number of MSCs to engraft at the lesion site of ischemia and reperfusion injury (Figure 5a). A similar trend in the MSC retention at the injury site was observed on day 14; the number of MSCs at the site increased by more than 7-fold in the MSC-GO group compared to the MSC group (Figure 5a). In addition, the MSC dispersion in the injury region notably changed on day 14 (Figure 5a). MSCs remained localized at the site of injection in the MSC-GO group (Figure 5a), which may be due to the strong adhesion of grafted MSCs at the lesion site, as demonstrated *in vitro* in Figure 3a. In addition, we examined the terminal deoxynucleotidyl transferase (TdT)-mediated dUTP nick-end labeling (TUNEL) expression of implanted MSCs to analyze their apoptotic activity. Significantly more MSCs were stained with TUNEL in the MSC group compared to the MSC-GO group (Figure 5b), which suggests that unmodified MSCs are more susceptible to ROS-mediated apoptosis, as demonstrated in the *in vitro* results.

Growing evidence suggests that the major mechanism of cardiac repair by stem cell implantation is reparative paracrine factor secretion from the implanted stem cells rather than the differentiation of the engrafted stem cells into cardiac cells.[48] In addition, although there are some controversies, it has been reported that electromechanical integration is incomplete following therapeutic cell implantation, as demonstrated by limited expression of adherens and gap junction proteins.[49,50] Therefore, in this study, we focused on the paracrine effect of implanted MSCs and MSC-GO after they survived in the infarcted region (Figure 5a) rather than their formation of adheren junctions with the host cells.

Paracrine factors promote angiogenesis in a dose-dependent manner in the ischemic regions, and this effect could be enhanced by increasing the number of implanted cells.[51] In this study, we have increased the number of MSCs engrafted in the ischemic heart by promoting their survival rather than administrating more MSCs (Figure 5a,b). The enhanced survival of MSCs significantly enhanced the secretion of pro-angiogenic growth factors, such as VEGF and FGF2, *in vitro* (Figure 3d). *In vivo*, the secretion of human VEGF by the implanted human MSCs was analyzed as an example for paracrine factor secretion. The secretion of VEGF was increased in the MSC-GO group (Figure 5c). By calculating the relative amount of VEGF secreted by each MSC, which did not significantly differ between MSCs and MSC-GO (Figure 5c), we demonstrated that the increased number of engrafted MSCs is responsible for the enhanced secretion of VEGF in the MSC-GO group. This finding also demonstrates that the biofunctionality of the implanted MSCs was preserved irrespective of the use of GO flakes.

Improvement in Myocardial Repair by MSC-GO. Previous studies have demonstrated that the secretion of pro-angiogenic growth factors contributes to the neovascularization in the ischemic myocardium and promotes myocardial repair.[41] In the present study, the enhanced growth factor secretion by MSC-GO enhanced the neovascularization in the infarcted region (Figure 6).

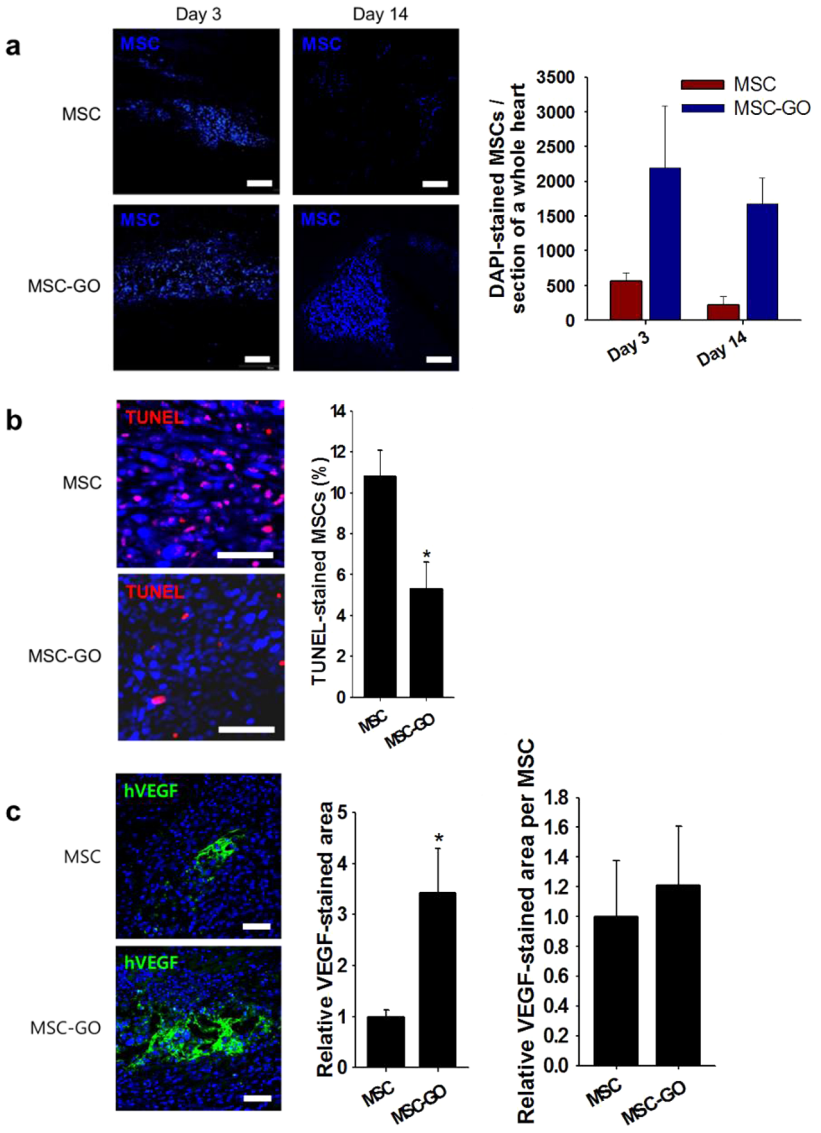

Figure 5. Survival and VEGF secretion from MSCs or MSC-GO implanted into the reperfused MI region evaluated by immunohistochemistry. (a) Detection of DAPI (blue)-labeled MSCs 3 and 14 days after MSC implantation. Scale bars, 100 μm. (b) TUNEL (red) staining 3 days after MSC implantation. The MSCs were labeled with DAPI (blue). Scale bars, 50 μm. (c) Human VEGF (green) staining 3 days after human MSC or human MSC-GO implantation. All cells (not only MSCs) were counterstained with DAPI (blue). Scale bars, 50 μm. *$p < 0.05$ compared to any group; $^{\#}p < 0.05$; $n = 3$.

The heart sections retrieved 14 days after cell implantation were stained for smooth muscle actin α (SMA-α) and von Willebrand Factor (vWF). To quantify the number of vessels in the infarcted region, arterioles were assigned as SMA-α-positive vessels and capillaries were assigned as vWF-positive minus SMA-α-positive vessels.[52] While MSCs could promote angiogenesis in the infarcted myocardium compared to the PBS injection group, MSC-GO could further enhance neovascularization (Figure 6).

Enhanced angiogenesis contributes to heart repair after MI.[53] The promotion of angiogenesis due to enhanced paracrine secretion by MSC-GO attenuated left ventricular remodeling (Figure 7).[54] Masson's trichrome staining and triphenyl tetrazolium chloride (TTC) staining were performed 14 days after the treatment to assess the area of collagen-containing fibrous tissue and infarcted left ventricle, respectively. The Masson's trichrome staining of the longitudinal sections of the heart showed a large fibrotic area (blue) in the PBS and MSC groups, while the fibrotic area was significantly smaller in the MSC-GO group (Figure 7a). TTC staining demonstrated that MSC-GO significantly decreased the infarction size (Figure 7b). TUNEL staining showed that the cardiac cells in the infarcted region of the PBS and MSC groups continued to undergo apoptosis (Figure 7c), which further aggravated the infarction. However, significantly fewer cells were stained with TUNEL in the MSC-GO group (Figure 7c), which demonstrated that the progress of infarction was slowed.

In vivo toxicity of GO flakes was not significant in this study even though GO flakes showed no sign of

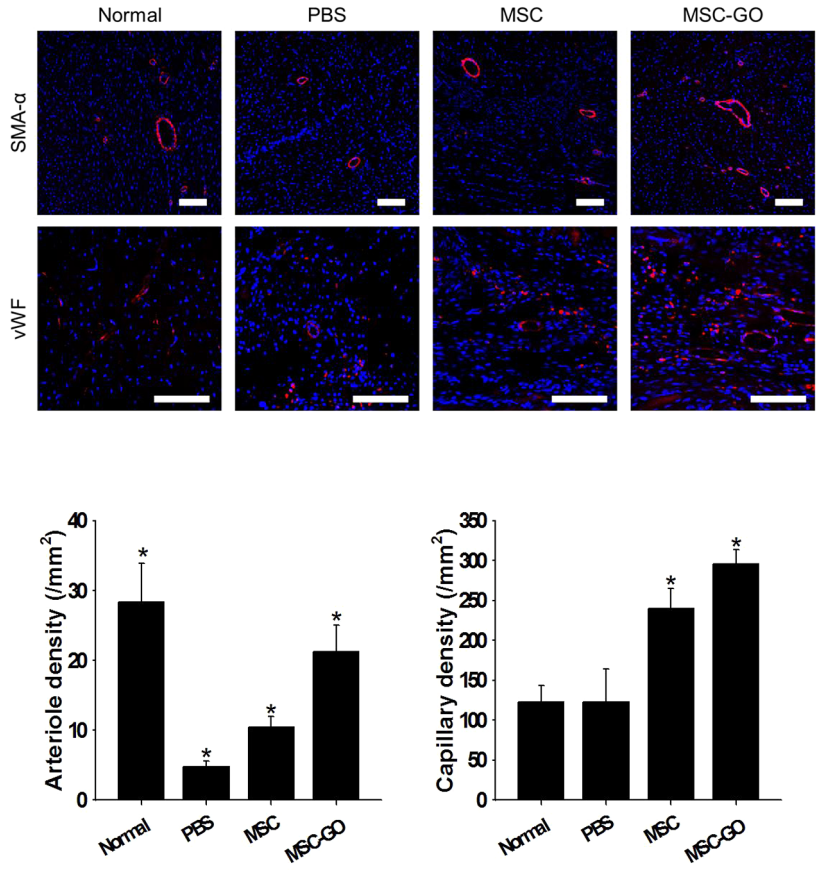

Figure 6. Microvessel density in the infarcted region 14 days after MSC or MSC-GO implantation. The arteriole densities were quantified by counting the SMA-α-positive (red) vessels. The capillary densities were quantified by subtracting the SMA-α-positive vessels from vWF-positive (red) vessels. *$p < 0.05$ compared to any group.

degradation 14 days after implantation (Supporting Information Figures S5 and S6). Previous studies have reported that the implantation of GO particles did not exhibit obvious *in vivo* toxicity.[55,56] Yang *et al.* have demonstrated that GO implanted into mice at a concentration of 50 mg/kg is retained in the body for more than 30 days, yet no significant toxicity was observed even after 90 days.[56] GO exhibits dose-dependent toxicity; GO implantation in mice at a dosage less than 100 mg/kg body weight does not elicit obvious toxicity.[57] In this study, a GO concentration of 10 μg/mL was not cytotoxic to MSCs *in vitro* (Figure 2f). For *in vivo* implantation, a GO dosage of 1 mg/kg body weight was used. We carried out a TUNEL assay at the site of cell implantation (peri-infarcted region rather than the infarcted region) to examine the toxic effects of GO on the surrounding cells, including the implanted MSCs and native heart cells. The TUNEL staining demonstrated that GO flakes did not induce significant apoptosis as a notable increase in TUNEL-stained cells was not detected near the GO flakes (Supporting Information Figure S5).

In addition to the TUNEL assay, we have carried out hematoxylin and eosin staining of the implantation site to assess inflammatory cell infiltration. Inflammation plays an important role in determining the foreign body response to the implanted materials.[58] The hematoxylin and eosin staining results showed that there were inflammatory cells in both MSC and MSC-GO groups, which is in accordance with previous studies that showed large amounts of inflammatory cell infiltration in the infarcted heart at day 14.[59,60] However, the implantation of MSC-GO did not significantly aggravate the inflammatory cell invasion compared to the implantation of MSCs alone (Supporting Information Figure S6), indicating that there was no significant foreign body response against the implanted GO flakes. A previous study has also demonstrated that a combination of GO and hydrogel injected into the peri-infarcted regions of the heart after MI induction did not stimulate inflammatory responses.[18] Therefore, although overcoming the long-time retention of GO flakes postimplantation *in vivo* remains a challenge, and this retention may not be of consequence for the *in vivo* use given appropriate doses.

The implantation of MSC-GO also improved cardiac function (Figure 8). The implantation of MSC-GO increased the number of engrafted MSCs and the amount of secreted paracrine factors, which enhanced angiogenesis and prevented further remodeling of the infarcted myocardium. The enhanced therapeutic angiogenesis and the inhibition of cardiomyocyte

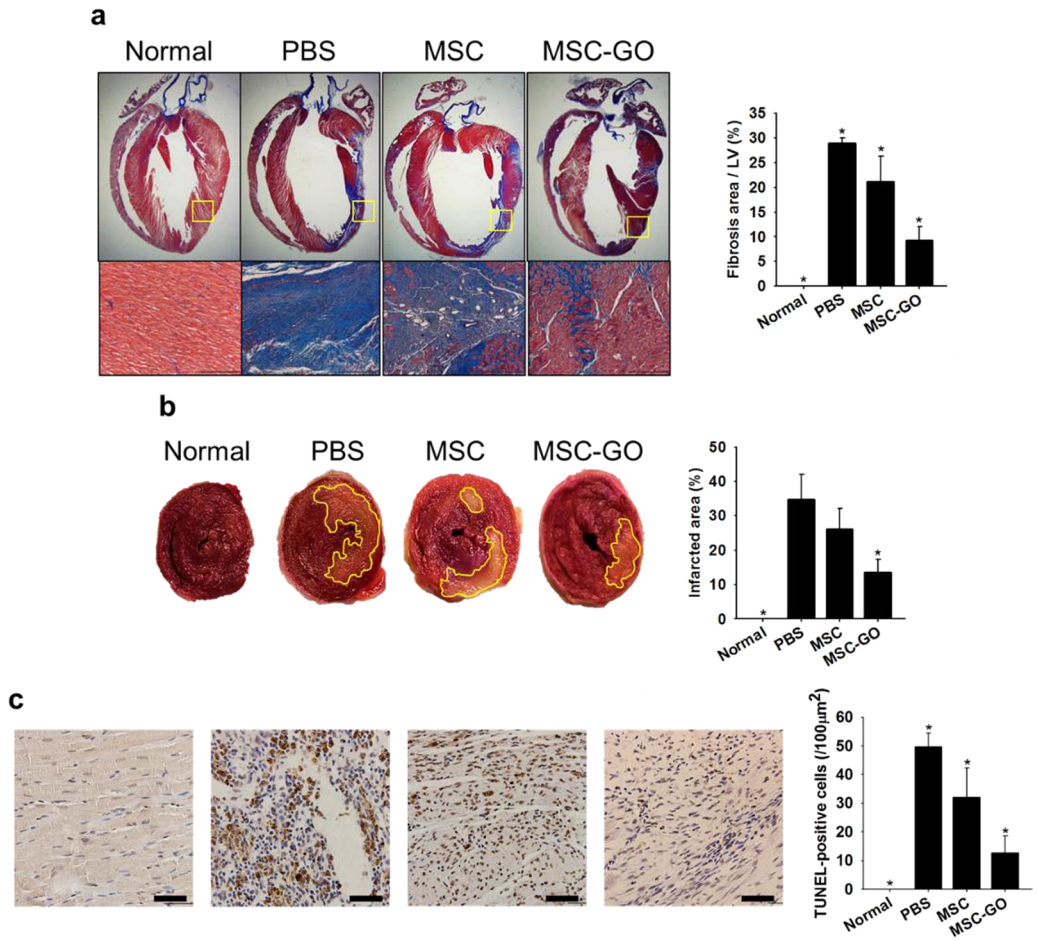

Figure 7. Enhanced cardiac repair by MSC-GO implantation (14 days after implantation). (a) Fibrosis evaluated based on a histological analysis with Masson's trichrome staining. Blue indicates fibrosis. (b) Infarcted area evaluated based on the TTC staining of heart sections. The infarcted area is marked with a yellow line. (c) Tissue apoptosis in the infarcted zone as evaluated by TUNEL staining (brown). Scale bars, 50 μm. *$p < 0.05$ compared to any group.

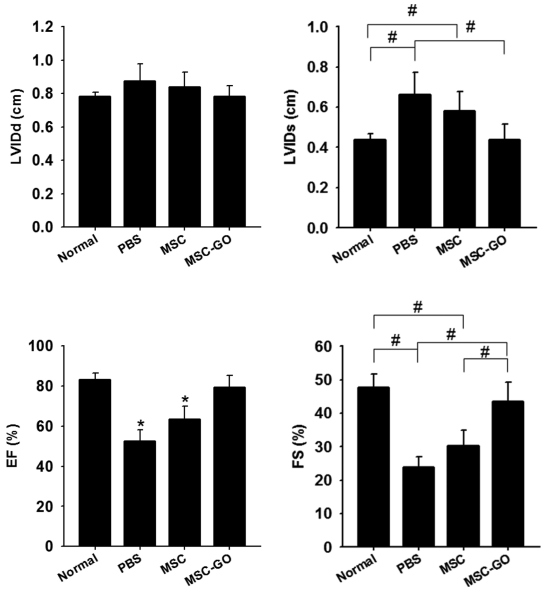

Figure 8. Heart functions and left ventricular size 14 days after treatments, as evaluated by echocardiography. *$p < 0.05$ compared to any group; $^{\#}p < 0.05$.

apoptosis contribute to the functional improvement of the infarcted heart.[61] Herein, a transthoracic echocardiograph showed that the left ventricular internal diameter at end diastole (LVIDd) did not significantly differ among groups (Figure 8). However, the implantation of MSC-GO markedly decreased the left ventricular internal diameter at end systole (LVIDs) compared to the PBS group, but this parameter did not significantly differ when compared with the normal group (Figure 8). In contrast, unmodified MSCs showed significantly larger LVIDs than the normal group (Figure 8). The left ventricular ejection fraction (EF) and fractional shortening (FS) were significantly enhanced in the MSC-GO group compared to the PBS and MSC groups and did not significantly differ from the normal group (Figure 8). In summary, the enhanced survival of implanted MSCs in the MSC-GO group resulted in enhanced paracrine factor secretion and reduced cardiac tissue apoptosis by promoting angiogenesis, attenuating the remodeling of the infarcted heart, and improving cardiac function after ischemia and reperfusion injury.

CONCLUSIONS

This study shows that GO flakes could effectively prevent a series of adverse cell-signaling cascades that result in the anoikis of MSCs in response to ROS that are generated in the ischemia-damaged and reperfused myocardium. This effect was due to the ability of GO flakes to provide a platform for MSC adhesion. The improved survival of MSCs following the implantation of MSC-GO into the infarcted and reperfused myocardium resulted in the enhanced secretion of reparative paracrine factors and reduced apoptosis of cardiac tissue, which enhanced angiogenesis and improved cardiac function. Therefore, GO may be utilized to protect therapeutic cells implanted into various ROS-abundant damaged tissues as part of stem cell implantation therapies for ischemic diseases after reperfusion.

METHODS

GO Preparation and Analyses. Graphite powder (<20 μm) was purchased from Sigma-Aldrich and used as received. GO was synthesized using a modified Hummers method.[62] The synthesized GO was suspended in water (0.05 wt %) to yield a brown dispersion. The GO was exfoliated by ultrasonication for 3 h, and the mixture was subsequently dialyzed (12−14 kDa cutoff) for 6 h to remove residual salts and acids. The obtained solution was then subjected to 20 min of centrifugation at 3000 rpm to remove the unexfoliated GO.

The samples were characterized by AFM, TEM, SAED, FTIR, ICP-MS, and Raman spectroscopy. The surface morphology of the samples was examined using the non-contact-mode AFM (XE-100 system, Park Systems, Korea). TEM and SAED were conducted on a TEM (JEOL 2100, JEOL, Japan) operated at 200 kV installed at the National Center for Interuniversity Research Facilities at Seoul National University. The rotation between the TEM images and corresponding SAED patterns was calibrated using molybdenum trioxide crystals. The FTIR spectra were obtained on a Fourier transform infrared spectrometer (Thermo Scientific Nicolet 6700 spectrometer). The samples for FTIR measurement were prepared by grinding the dried GO powder. The structural properties of GO flakes were further investigated by Raman spectroscopy (RM 1000-Invia, Renishaw, UK). The heavy metal content in GO was measured using ICP-MS (820-MS, Varian, Mulgrave, Australia). The Raman spectra were recorded by using an argon ion laser (514 nm) as the excitation source with a notch filter of 50 cm^{-1}. Typical scan ranged from 1000 to 3000 cm^{-1}, and the instrumental resolution was 10 cm^{-1}.

Culture of MSCs. Human bone marrow MSCs were purchased from Lonza (Walkersville, MD, USA). The MSCs were cultured Dulbecco's modified Eagle medium (DMEM, Gibco, NY, USA) supplemented with 10% (v/v) fetal bovine serum (FBS), 100 units/mL penicillin, and 100 μg/mL streptomycin. MSCs at passage 6 were used for this study. To prepare the MSC-GO, GO flakes were added to the culture medium and allowed to adhere to MSCs for 24 h. The cytotoxicity of GO was measured using cell counting kit-8 (CCK-8, Dojindo Laboratories, Kumamoto, Japan). Three samples were analyzed per group.

Analyses of GO Adhesion on MSCs. GO flakes were labeled with DiI (1 μg/mL, Sigma) for 12 h at 37 °C. After being labeled, the MSCs were labeled with DAPI (Sigma) and PKH67 (Sigma) according to the manufacturer's instructions. The GO flakes and MSCs were washed three times with PBS. GO flakes (10 μg/mL) were added to the MSC culture, and the GO flakes were allowed to adhere to MSCs for 24 h. The cells were collected by trypsinization and analyzed with fluorescent microscopy (model IX71, Olympus, Tokyo, Japan). After trypsinization, the cells were examined under a fluorescent microscope to ensure that none of the GO flakes had detached. The adhesion of GO to the MSCs was analyzed using TEM. First, the MSC-GO was fixed with Karnovsky's solution (EMS Hatfield, PA, USA) for 24 h at 4 °C and washed three times with a 0.05 M sodium cacodylate buffer. The specimens were then fixed with 2% osmium tetroxide (sigma) for 2 h at 4 °C, washed three times with cold distilled water, dehydrated using a series of graded ethanol and propylene oxide rinses, and finally embedded in Spurr's resin. The samples were then polymerized at 60 °C for 24 h and sectioned using an ultramicrotome (MTX, RMC, Arizona, USA). The thin sections were observed with a Libra 120 microscope (Carl Zeiss, Oberkochen, Germany).

Assays for Cell Adhesion and Viability with or without GO. The MSCs and MSC-GO were seeded on cell culture plates in the presence of 0 or 200 μM H_2O_2, an exogenous ROS source. The number of live cells was determined by CCK-8 after 90 min and 24 h according to the manufacturer's protocol (n = 3 per group). The adhesion of the cells was visualized with rhodamine-conjugated phalloidin (Millipore).

To determine the effect of GO flakes on the prevention of cell anoikis, MSCs and MSC-GO were plated on agar-coated plates, which prevents cell adhesion to the plate. The number of live cells was determined by CCK-8 after 24 h (n = 3 per group).

Detection of ROS. The amount of ROS is detected using a hydrogen peroxide assay kit (Biovision, CA, USA) according to the manufacturer's instructions (n = 4). The intracellular ROS was detected by staining cells with DCFDA (10 μM, Sigma) for 30 min.

qRT-PCR Analysis. Ribonucleic acid (RNA) samples were extracted using a Qiagen RNeasy mini kit according to the manufacturer's instructions (Qiagen, Germany). The total RNA concentration was determined using a NanoDrop spectrometer (ND-2000, NanoDrop Technologies, USA). Five hundred nanograms of total RNA from each sample was reverse-transcribed into cDNA using GoScript reverse transcriptase (Promega, USA). SYBR Green-based qRT-PCR was performed using a StepOnePlus real-time PCR system (Applied Biosystems, USA) instrument with TOPreal qPCR premix (Enzynomics, Korea). After 10 min of preincubation, 40 amplification cycles were performed, and each cycle consisted of three steps: 30 s at 94 °C, 45 s at 55 °C, and 45 s at 72 °C. The primer sequences for qRT-PCR are listed in Table S1, Supporting Information. All data were analyzed using the $2^{-\Delta\Delta Ct}$ method.

Western Blot Analysis. The protein expression was analyzed using 10% (w/v) SDS (sodium dodecyl sulfate)-polyacrylamide gel electrophoresis (n = 3 per group). The proteins were first transferred to an Immobilon-P membrane (Millipore Corp., USA) and then probed with antibodies against FN, pFAK, FAK, pp38, p38, caspase-3, and β-actin (all purchased from Abcam, UK). The proteins were then incubated with a horseradish-peroxidase-conjugated secondary antibody (Santa Cruz Biotechnology, USA) for 1 h at room temperature. The blots were developed using an enhanced chemiluminescence detection system (Amersham Bioscience, USA).

Adhesion of FN- or VN-Adsorbed GO Flakes to MSCs. To adsorb FN or VN on GO, GO flakes (10 μg/mL) were incubated with FN (50 μg/mL) or VN (50 μg/mL) in PBS for 3 h.[23] Unbound FN and VN were removed by washing with PBS for three times. FN- or VN-adsorbed GO flakes (10 μg/mL) were added to the MSC culture and allowed to adhere to MSCs for 24 h.

Competition between Free ECM Proteins and ECM Proteins Adsorbed on GO for Their Interactions with MSCs. MSCs were incubated with ECM protein-adsorbed and DiI-labeled GO flakes in serum-free medium or serum-containing medium for 24 h. The serum-containing medium contains free ECM proteins. Unbound GO flakes were removed by washing several times with PBS. ECM protein-adsorbed GO flakes were also incubated in serum-free medium and serum-containing medium without MSCs for 24 h in order to confirm GO attachment to MSCs rather than the dish. The adhesion of GO flakes to MSCs was analyzed with fluorescent microscopy.

ELISA. After the MSCs were allowed to attach to the cell culture plate containing 10% (v/v) serum-containing medium for 24 h, the medium was changed to DMEM without FBS for 24 h. The amount of growth factors in the supernatant was then measured using an ELISA assay kit (n = 3 per group, R&D Systems, Minneapolis, MN, USA).

Induction of Myocardial Infarction and Treatment. Myocardial infarction was induced in 8-week-old Sprague−Dawley rats (n = 16 per group, 240 ± 10 g, Samtako Bio, Osan, Korea) as previously described.[63] Briefly, the rats were placed under general anesthesia, and the heart was exposed at the left costal rib using an incision. The left anterior descending artery was ligated with a 6−0 silk suture (Ethicon, Cincinnati, OH, USA) for 1 h and then reperfused. The infarction was macroscopically visualized as blanching in the left ventricle. No ligation was performed for the normal group. The animals were sacrificed 14 days after the implantation unless stated otherwise. The animals were used in accordance with the International Guide for the Care and Use of Laboratory Animals. The experimental protocol was approved by the Animal Research Committee of Yonsei University College of Medicine (IACUC No. 2012-0202-2).

MSC Labeling and Implantation. To track MSCs *in vivo*, the MSCs were labeled with DAPI by adding DAPI solution to the culture medium according to the manufacturer's instruction. One million MSCs were suspended in 60 μL of PBS and injected using a 30 guage needle after reperfusion at the anterior and lateral aspects of the infarction border zone. For the PBS injection, 60 μL of PBS was injected at the same sites. The site of injection was examined to analyze surviving cells, and the infarction site was examined to assess cardiac regeneration.

Analyses of Surviving MSCs. The animals were sacrificed 3 or 14 days after cell implantation. The heart tissues were fixed with 10% (v/v) formaldehyde, embedded in paraffin, and sliced into 5 μm sections. The sections were deparaffinized and rehydrated. A TUNEL assay was performed to detect the apoptotic activity in the implanted MSCs using an ApopTag Red *in situ* apoptosis detection kit (Millipore) according to the manufacturer's instruction. Four separate slides were photographed using a fluorescent microscope, and DAPI-labeled cells and TUNEL-positive cells were counted (n = 3 hearts per group).

The amount of human VEGF secreted by implanted human MSCs was determined by staining tissue sections with anti-VEGF antibody (ab52917, Abcam) that reacts specifically with human VEGF. VEGF fluorescently stained using a FITC secondary antibody (Jackson ImmunoResearch Laboratories, n = 3 hearts per group).

Analyses of Arteriole and Capillary Density. The arteriole and capillary density were evaluated using SMA-α (Abcam) and vWF (Abcam) staining, respectively. The bound vWF and SMA-α were visualized by staining with a rhodamine-conjugated secondary antibody (Jackson ImmunoResearch Laboratories, n = 3 hearts per group).

Histology. To assess the formation of fibrotic tissue after infarction, the heart sections were stained with Masson's trichrome and hematoxylin and eosin. The size of the area of fibrotic tissue was measured using the MetaMorph software (Molecular Devices, Sunnyvale, CA) and is expressed as the percentage of the total left ventricle. To measure the infarcted size of the myocardium, the rat hearts were transaxially sectioned and incubated in TTC (Sigma) for 20 min at 37 °C, followed by 10% (v/v) formalin fixation at 2−8 °C overnight. The infarcted region appeared yellow-white, and the viable myocardium appeared red. The heart sections were photographed with a digital camera, and the area was measured using planimetry and the ImageJ software (National Institutes of Health, Bethesda, MD, USA). The area of the infarction is expressed as the percentage of yellow-white infarcted tissue to the total left ventricle. Three heart samples per group were used for the analyses. A TUNEL assay was performed to detect the apoptotic activity in the implanted MSCs using an ApopTag peroxidase *in situ* apoptosis detection kit (Millipore) according to the manufacturer's instructions.

Evaluation of Cardiac Function. A two-dimensional transthoracic echocardiograph was performed at baseline (normal) and for all experimental groups (n = 5 rats per group) 14 days after treatment. An experienced cardiologist, blinded to the identity of the experimental groups, carried out the assessments. Echocardiography analyses were performed on a GE Vivid Seven ultrasound machine (GE Medical System, Fairfield, CT) using a 10.0 MHz transducer, and the data from the digital pictures of the short-axis views were analyzed.

Statistical Analysis. The quantitative data were expressed as the means ± standard deviations. The statistical analysis was performed using one-way analysis of variance (ANOVA) with the Tukey significant difference post hoc test using SPSS software (SPSS Inc., USA). A value of $p < 0.05$ was considered to denote statistical significance.

Conflict of Interest: The authors declare no competing financial interest.

Acknowledgment. This research was supported by a grant (2014029716) from the National Research Foundation of Korea and grants (HI12C0199 and HI14C1550) from the Korea Health Industry Development Institute (KHIDI), as funded by the Ministry of Health and Welfare, Republic of Korea.

Supporting Information Available: Figures S1−S6 and Table S1. The Supporting Information is available free of charge on the ACS Publications website at DOI: 10.1021/nn507149w.

REFERENCES AND NOTES

1. Lloyd-Jones, D.; Adams, R. J.; Brown, T. M.; Carnethon, M.; Dai, S.; De Simone, G.; Ferguson, T. B.; Ford, E.; Furie, K.; Gillespie, C.; et al. Heart Disease and Stroke Statistics—2010 Update: A Report from the American Heart Association. *Circulation* **2010**, *121*, e46–e215.
2. Tofield, A. European Cardiovascular Disease Statistics 2012 Summary. *Eur. Heart J.* **2013**, *34*, 1086–1086.
3. Thygesen, K.; Alpert, J. S.; Jaffe, A. S.; Simoons, M. L.; Chaitman, B. R.; White, H. D.; Force, J. E. A. A. W. T. Third Universal Definition of Myocardial Infarction. *Rev. Esp. Cardiol.* **2013**, *66*, 2551–2567.
4. Orlic, D.; Kajstura, J.; Chimenti, S.; Jakoniuk, I.; Anderson, S. M.; Li, B.; Pickel, J.; McKay, R.; Nadal-Ginard, B.; Bodine, D. M.; et al. Bone Marrow Cells Regenerate Infarcted Myocardium. *Nature* **2001**, *410*, 701–705.
5. Kinnaird, T.; Stabile, E.; Burnett, M. S.; Lee, C. W.; Barr, S.; Fuchs, S.; Epstein, S. E. Marrow-Derived Stromal Cells Express Genes Encoding a Broad Spectrum of Arteriogenic Cytokines and Promote in Vitro and in Vivo Arteriogenesis through Paracrine Mechanisms. *Circ. Res.* **2004**, *94*, 678–685.
6. Lee, W. Y.; Wei, H. J.; Lin, W. W.; Yeh, Y. C.; Hwang, S. M.; Wang, J. J.; Tsai, M. S.; Chang, Y.; Sung, H. W. Enhancement of Cell Retention and Functional Benefits in Myocardial Infarction Using Human Amniotic-Fluid Stem-Cell Bodies Enriched with Endogenous ECM. *Biomaterials* **2011**, *32*, 5558–5567.
7. Terrovitis, J.; Lautamaki, R.; Bonios, M.; Fox, J.; Engles, J. M.; Yu, J.; Leppo, M. K.; Pomper, M. G.; Wahl, R. L.; Seidel, J.; et al. Noninvasive Quantification and Optimization of Acute Cell Retention by in Vivo Positron Emission Tomography after Intramyocardial Cardiac-Derived Stem Cell Delivery. *J. Am. Coll. Cardiol.* **2009**, *54*, 1619–1626.
8. Eltzschig, H. K.; Eckle, T. Ischemia and Reperfusion—From Mechanism to Translation. *Nat. Med.* **2011**, *17*, 1391–1401.
9. Angelos, M. G.; Kutala, V. K.; Torres, C. A.; He, G. L.; Stoner, J. D.; Mohammad, M.; Kuppusamy, P. Hypoxic Reperfusion of the Ischemic Heart and Oxygen Radical Generation. *Am. J. Physiol.* **2006**, *290*, H341–H347.
10. Gailit, J.; Colflesh, D.; Rabiner, I.; Simone, J.; Goligorsky, M. S. Redistribution and Dysfunction of Integrins in Cultured Renal Epithelial Cells Exposed to Oxidative Stress. *Am. J. Physiol.* **1993**, *264*, F149–F157.
11. Chiarugi, P.; Giannoni, E. Anoikis: A Necessary Death Program for Anchorage-Dependent Cells. *Biochem. Pharmacol.* **2008**, *76*, 1352–1364.
12. Song, H.; Cha, M. J.; Song, B. W.; Kim, I. K.; Chang, W.; Lim, S.; Choi, E. J.; Ham, O.; Lee, S. Y.; Chung, N.; et al. Reactive Oxygen Species Inhibit Adhesion of Mesenchymal Stem

Cells Implanted into Ischemic Myocardium via Interference of Focal Adhesion Complex. *Stem Cells* **2010**, *28*, 555–563.
13. Dreyer, D. R.; Park, S.; Bielawski, C. W.; Ruoff, R. S. The Chemistry of Graphene Oxide. *Chem. Soc. Rev.* **2010**, *39*, 228–240.
14. Cha, C. Y.; Shin, S. R.; Gao, X. G.; Annabi, N.; Dokmeci, M. R.; Tang, X. W.; Khademhosseini, A. Controlling Mechanical Properties of Cell-Laden Hydrogels by Covalent Incorporation of Graphene Oxide. *Small* **2014**, *10*, 514–523.
15. Kanakia, S.; Toussaint, J. D.; Chowdhury, S. M.; Lalwani, G.; Tembulkar, T.; Button, T.; Shroyer, K. R.; Moore, W.; Sitharaman, B. Physicochemical Characterization of a Novel Graphene-Based Magnetic Resonance Imaging Contrast Agent. *Int. J. Nanomed.* **2013**, *8*, 2821–2833.
16. Lalwani, G.; Sundararaj, J. L.; Schaefer, K.; Button, T.; Sitharaman, B. Synthesis, Characterization, in Vitro Phantom Imaging, and Cytotoxicity of a Novel Graphene-Based Multimodal Magnetic Resonance Imaging-X-ray Computed Tomography Contrast Agent. *J. Mater. Chem. B* **2014**, *2*, 3519–3530.
17. Liu, J. Q.; Cui, L.; Losic, D. Graphene and Graphene Oxide as New Nanocarriers for Drug Delivery Applications. *Acta Biomater.* **2013**, *9*, 9243–9257.
18. Paul, A.; Hasan, A.; Al Kindi, H.; Gaharwar, A. K.; Rao, V. T. S.; Nikkhah, M.; Shin, S. R.; Krafft, D.; Dokmeci, M. R.; Shum-Tim, D.; et al. Injectable Graphene Oxide/Hydrogel-Based Angiogenic Gene Delivery System for Vasculogenesis and Cardiac Repair. *ACS Nano* **2014**, *8*, 8050–8062.
19. Feng, L.; Zhang, S.; Liu, Z. Graphene Based Gene Transfection. *Nanoscale* **2011**, *3*, 1252–1257.
20. Shin, S. R.; Aghaei-Ghareh-Bolagh, B.; Gao, X.; Nikkhah, M.; Jung, S. M.; Dolatshahi-Pirouz, A.; Kim, S. B.; Kim, S. M.; Dokmeci, M. R.; Tang, X.; et al. Layer-by-Layer Assembly of 3d Tissue Constructs with Functionalized Graphene. *Adv. Funct. Mater.* **2014**, *24*, 6136–6144.
21. Shen, H.; Zhang, L.; Liu, M.; Zhang, Z. Biomedical Applications of Graphene. *Theranostics* **2012**, *2*, 283–294.
22. Lee, W. C.; Lim, C. H.; Shi, H.; Tang, L. A.; Wang, Y.; Lim, C. T.; Loh, K. P. Origin of Enhanced Stem Cell Growth and Differentiation on Graphene and Graphene Oxide. *ACS Nano* **2011**, *5*, 7334–7341.
23. Shi, X. T.; Chang, H. X.; Chen, S.; Lai, C.; Khademhosseini, A.; Wu, H. K. Regulating Cellular Behavior on Few-Layer Reduced Graphene Oxide Films with Well-Controlled Reduction States. *Adv. Funct. Mater.* **2012**, *22*, 751–759.
24. Grinnell, F.; Feld, M. K. Fibronectin Adsorption on Hydrophilic and Hydrophobic Surfaces Detected by Antibody-Binding and Analyzed during Cell-Adhesion in Serum-Containing Medium. *J. Biol. Chem.* **1982**, *257*, 4888–4893.
25. Marcano, D. C.; Kosynkin, D. V.; Berlin, J. M.; Sinitskii, A.; Sun, Z. Z.; Slesarev, A.; Alemany, L. B.; Lu, W.; Tour, J. M. Improved Synthesis of Graphene Oxide. *ACS Nano* **2010**, *4*, 4806–4814.
26. Peng, L.; Xu, Z.; Liu, Z.; Wei, Y. Y.; Sun, H. Y.; Li, Z.; Zhao, X. L.; Gao, C. An Iron-Based Green Approach to 1-H Production of Single-Layer Graphene Oxide. *Nat. Commun.* **2015**, *6*, 5716.
27. Chang, Y.; Yang, S. T.; Liu, J. H.; Dong, E.; Wang, Y.; Cao, A.; Liu, Y.; Wang, H. In Vitro Toxicity Evaluation of Graphene Oxide on A549 Cells. *Toxicol. Lett.* **2011**, *200*, 201–210.
28. Wojtoniszak, M.; Chen, X.; Kalenczuk, R. J.; Wajda, A.; Lapczuk, J.; Kurzewski, M.; Drozdzik, M.; Chu, P. K.; Borowiak-Palen, E. Synthesis, Dispersion, and Cytocompatibility of Graphene Oxide and Reduced Graphene Oxide. *Colloids Surf., B* **2012**, *89*, 79–85.
29. Treossi, E.; Melucci, M.; Liscio, A.; Gazzano, M.; Samori, P.; Palermo, V. High-Contrast Visualization of Graphene Oxide on Dye-Sensitized Glass, Quartz, and Silicon by Fluorescence Quenching. *J. Am. Chem. Soc.* **2009**, *131*, 15576–15577.
30. Yoon, H. H.; Bhang, S. H.; Kim, T.; Yu, T.; Hyeon, T.; Kim, B.-S. Dual Roles of Graphene Oxide in Chondrogenic Differentiation of Adult Stem Cells: Cell-Adhesion Substrate and Growth Factor-Delivery Carrier. *Adv. Funct. Mater.* **2014**, n/a–n/a.
31. Sinoforoglu, M.; Gur, B.; Arik, M.; Onganer, Y.; Meral, K. Graphene Oxide Sheets as a Template for Dye Assembly: Graphene Oxide Sheets Induce H-Aggregates of Pyronin (Y) Dye. *RSC Adv.* **2013**, *3*, 11832–11838.
32. Talukdar, Y.; Rashkow, J. T.; Lalwani, G.; Kanakia, S.; Sitharaman, B. The Effects of Graphene Nanostructures on Mesenchymal Stem Cells. *Biomaterials* **2014**, *35*, 4863–4877.
33. Chowdhury, S. M.; Lalwani, G.; Zhang, K. V.; Yang, J. Y.; Neville, K.; Sitharaman, B. Cell Specific Cytotoxicity and Uptake of Graphene Nanoribbons. *Biomaterials* **2013**, *34*, 283–293.
34. Ma, N.; Ma, C.; Li, C.; Wang, T.; Tang, Y.; Wang, H.; Moul, X.; Chen, Z.; Hel, N. Influence of Nanoparticle Shape, Size, and Surface Functionalization on Cellular Uptake. *J. Nanosci. Nanotechnol.* **2013**, *13*, 6485–6498.
35. Kim, J.; Choi, K. S.; Kim, Y.; Lim, K. T.; Seonwoo, H.; Park, Y.; Kim, D. H.; Choung, P. H.; Cho, C. S.; Kim, S. Y.; et al. Bioactive Effects of Graphene Oxide Cell Culture Substratum on Structure and Function of Human Adipose-Derived Stem Cells. *J. Biomed. Mater. Res., Part A* **2013**, *101*, 3520–3530.
36. Gnecchi, M.; He, H.; Liang, O. D.; Melo, L. G.; Morello, F.; Mu, H.; Noiseux, N.; Zhang, L.; Pratt, R. E.; Ingwall, J. S.; et al. Paracrine Action Accounts for Marked Protection of Ischemic Heart by Akt-Modified Mesenchymal Stem Cells. *Nat. Med.* **2005**, *11*, 367–368.
37. Martinez, E. C.; Kofidis, T. Adult Stem Cells for Cardiac Tissue Engineering. *J. Mol. Cell. Cardiol.* **2011**, *50*, 312–319.
38. Liu, P.; Hock, C. E.; Nagele, R.; Wong, P. Y. Formation of Nitric Oxide, Superoxide, and Peroxynitrite in Myocardial Ischemia-Reperfusion Injury in Rats. *Am. J. Physiol.* **1997**, *272*, H2327–H2336.
39. Zhang, Z. Y.; Turner, D. C.; Drzewiecki, G. J.; Hinshaw, D. B.; Hyslop, P. A. Impairment of Integrin-Mediated Cell-Matrix Adhesion in Oxidant-Stressed Pc12 Cells. *Brain Res.* **1994**, *662*, 189–197.
40. Bhang, S. H.; Lee, T. J.; La, W. G.; Kim, D. I.; Kim, B. S. Delivery of Fibroblast Growth Factor 2 Enhances the Viability of Cord Blood-Derived Mesenchymal Stem Cells Transplanted to Ischemic Limbs. *J. Biosci. Bioeng.* **2011**, *111*, 584–589.
41. Tang, Y. L.; Zhao, Q.; Zhang, Y. C.; Cheng, L.; Liu, M.; Shi, J.; Yang, Y. Z.; Pan, C.; Ge, J.; Phillips, M. I. Autologous Mesenchymal Stem Cell Transplantation Induce VEGF and Neovascularization in Ischemic Myocardium. *Regul. Pept.* **2004**, *117*, 3–10.
42. Rosen, K.; Shi, W.; Calabretta, B.; Filmus, J. Cell Detachment Triggers P38 Mitogen-Activated Protein Kinase-Dependent Overexpression of Fas Ligand—A Novel Mechanism of Anoikis of Intestinal Epithelial Cells. *J. Biol. Chem.* **2002**, *277*, 46123–46130.
43. Wei, H.; Li, Z. W.; Hu, S. S.; Chen, X.; Cong, X. F. Apoptosis of Mesenchymal Stem Cells Induced by Hydrogen Peroxide Concerns Both Endoplasmic Reticulum Stress and Mitochondrial Death Pathway through Regulation of Caspases, P38 and JNK. *J. Cell. Biochem.* **2010**, *111*, 967–978.
44. Hynes, R. O. Integrins: Versatility, Modulation, and Signaling in Cell Adhesion. *Cell* **1992**, *69*, 11–25.
45. Simon, H. U.; Haj-Yehia, A.; Levi-Schaffer, F. Role of Reactive Oxygen Species (ROS) in Apoptosis Induction. *Apoptosis* **2000**, *5*, 415–418.
46. Underwood, P. A.; Bennett, F. A. A Comparison of the Biological-Activities of the Cell-Adhesive Proteins Vitronectin and Fibronectin. *J. Cell Sci.* **1989**, *93*, 641–649.
47. Qiu, Y.; Wang, Z. Y.; Owens, A. C. E.; Kulaots, I.; Chen, Y. T.; Kane, A. B.; Hurt, R. H. Antioxidant Chemistry of Graphene-Based Materials and Its Role in Oxidation Protection Technology. *Nanoscale* **2014**, *6*, 11744–11755.
48. Mirotsou, M.; Jayawardena, T. M.; Schmeckpeper, J.; Gnecchi, M.; Dzau, V. J. Paracrine Mechanisms of Stem Cell Reparative and Regenerative Actions in the Heart. *J. Mol. Cell. Cardiol.* **2011**, *50*, 280–289.
49. Laflamme, M. A.; Murry, C. E. Regenerating the Heart. *Nat. Biotechnol.* **2005**, *23*, 845–856.
50. Reinecke, H.; Poppa, V.; Murry, C. E. Skeletal Muscle Stem Cells Do Not Transdifferentiate into Cardiomyocytes after Cardiac Grafting. *J. Mol. Cell. Cardiol.* **2002**, *34*, 241–249.

51. Kinnaird, T.; Stabile, E.; Burnett, M. S.; Shou, M.; Lee, C. W.; Barr, S.; Fuchs, S.; Epstein, S. E. Local Delivery of Marrow-Derived Stromal Cells Augments Collateral Perfusion through Paracrine Mechanisms. *Circulation* **2004**, *109*, 1543–1549.
52. Van't Hof, W.; Mal, N.; Huang, Y.; Zhang, M.; Popovic, Z.; Forudi, F.; Deans, R.; Penn, M. S. Direct Delivery of Syngeneic and Allogeneic Large-Scale Expanded Multipotent Adult Progenitor Cells Improves Cardiac Function after Myocardial Infarct. *Cytotherapy* **2007**, *9*, 477–487.
53. Ma, N.; Stamm, C.; Kaminski, A.; Li, W.; Kleine, H. D.; Muller-Hilke, B.; Zhang, L.; Ladilov, Y.; Egger, D.; Steinhoff, G. Human Cord Blood Cells Induce Angiogenesis Following Myocardial Infarction in Nod/Scid-Mice. *Cardiovasc. Res.* **2005**, *66*, 45–54.
54. Uemura, R.; Xu, M.; Ahmad, N.; Ashraf, M. Bone Marrow Stem Cells Prevent Left Ventricular Remodeling of Ischemic Heart through Paracrine Signaling. *Circ. Res.* **2006**, *98*, 1414–1421.
55. Kanakia, S.; Toussaint, J. D.; Mullick Chowdhury, S.; Tembulkar, T.; Lee, S.; Jiang, Y. P.; Lin, R. Z.; Shroyer, K. R.; Moore, W.; Sitharaman, B. Dose Ranging, Expanded Acute Toxicity and Safety Pharmacology Studies for Intravenously Administered Functionalized Graphene Nanoparticle Formulations. *Biomaterials* **2014**, *35*, 7022–7031.
56. Yang, K.; Gong, H.; Shi, X. Z.; Wan, J. M.; Zhang, Y. J.; Liu, Z. In Vivo Biodistribution and Toxicology of Functionalized Nano-Graphene Oxide in Mice after Oral and Intraperitoneal Administration. *Biomaterials* **2013**, *34*, 2787–2795.
57. Wang, K.; Ruan, J.; Song, H.; Zhang, J. L.; Wo, Y.; Guo, S. W.; Cui, D. X. Biocompatibility of Graphene Oxide. *Nanoscale Res. Lett.* **2011**, *6*, 8.
58. Gerullis, H.; Georgas, E.; Boros, M.; Klosterhalfen, B.; Eimer, C.; Arndt, C.; Otto, S.; Barski, D.; Ysebaert, D.; Ramon, A.; et al. Inflammatory Reaction as Determinant of Foreign Body Reaction Is an Early and Susceptible Event after Mesh Implantation. *Biomed Res. Int.* **2014**, 510807.
59. Morales, C.; Gonzalez, G. E.; Rodriguez, M.; Bertolasi, C. A.; Gelpi, R. J. Histopathologic Time Course of Myocardial Infarct in Rabbit Hearts. *Cardiovasc. Pathol.* **2002**, *11*, 339–345.
60. Takemura, G.; Ohno, M.; Hayakawa, Y.; Misao, J.; Kanoh, M.; Ohno, A.; Uno, Y.; Minatoguchi, S.; Fujiwara, T.; Fujiwara, H. Role of Apoptosis in the Disappearance of Infiltrated and Proliferated Interstitial Cells after Myocardial Infarction. *Circ. Res.* **1998**, *82*, 1130–1138.
61. Takahashi, M.; Li, T.-S.; Suzuki, R.; Kobayashi, T.; Ito, H.; Ikeda, Y.; Matsuzaki, M.; Hamano, K. Cytokines Produced by Bone Marrow Cells Can Contribute to Functional Improvement of the Infarcted Heart by Protecting Cardiomyocytes from Ischemic Injury. *Am. J. Physiol.* **2006**, *291*, H886–H893.
62. Hummers, W. S.; Offeman, R. E. Preparation of Graphitic Oxide. *J. Am. Chem. Soc.* **1958**, *80*, 1339–1339.
63. Chang, W.; Song, B. W.; Lim, S.; Song, H.; Shim, C. Y.; Cha, M. J.; Ahn, D. H.; Jung, Y. G.; Lee, D. H.; Chung, J. H.; et al. Mesenchymal Stem Cells Pretreated with Delivered Hph-1-Hsp70 Protein Are Protected from Hypoxia-Mediated Cell Death and Rescue Heart Functions from Myocardial Injury. *Stem Cells* **2009**, *27*, 2283–2292.